Explainable multi-view framework for dissecting inter-cellular signaling from highly multiplexed spatial data

Jovan Tanevski[1,2], Attila Gabor[1], Ricardo Omar Ramirez Flores[1], Denis Schapiro[3,4], Julio Saez-Rodriguez[1,5,*]

[1] Institute for Computational Biomedicine, Faculty of Medicine, Heidelberg University and Heidelberg University Hospital, Heidelberg, Germany

[2] Department of Knowledge Technologies, Jožef Stefan Institute, Ljubljana, Slovenia

[3] Laboratory of Systems Pharmacology, Harvard Medical School, Boston, MA, USA

[4] Klarman Cell Observatory, Broad Institute of MIT and Harvard, Cambridge, MA, USA

[5]Joint Research Centre for Computational Biomedicine (JRC-COMBINE), Faculty of Medicine, RWTH Aachen University, Aachen, Germany

* Corresponding author: julio.saez@bioquant.uni-heidelberg.de

Abstract

The advancement of technologies to measure highly multiplexed spatial data requires the development of scalable methods that can leverage the spatial information. We present MISTy, a flexible, scalable and explainable machine learning framework for extracting interactions from spatial omics data. MISTy builds multiple views focusing on different spatial or functional contexts to dissect different effects, such as those from direct neighbours versus those from distant cells. MISTy can be applied to different spatially resolved -omics data with dozens to thousands of markers. We evaluate the performance of MISTy on an *in silico* dataset and demonstrate its applicability on two breast cancer datasets measured with imaging mass cytometry and spatial transcriptomics, respectively. We show the relevance of the information extracted when separating the effect of close and distant cells. Finally, we demonstrate the integration of activities of pathways estimated in a spatial context for the analysis of intercellular signaling.

Keywords: spatial omics, multiplexed data, machine learning, intercellular signaling

Introduction

Highly multiplexed, spatially resolved data at single cell resolution is becoming available at an increasing pace thanks to recent and ongoing technical developments. In contrast to dissociated single-cell data, this data informs us on the cell-to-cell heterogeneity in tissue slices while conserving the arrangement of cells[1]. Therefore, each cell can be studied in its microenvironment. We can observe the spatial distribution of the expression of markers of interest, their interactions within the local cellular niche and at the level of tissue structure. All these aspects provide an excellent platform to gain better insight into multi-cellular processes, in particular cell-cell communication.

The proliferation of spatial technologies leads to the generation of large amounts of data. Different technologies allow for measuring different types of molecules with varying resolution, capturing different areas of tissue with diverse numbers of readouts. Immunofluorescence-based methods allow detection of the expression of tens to hundreds of proteins at subcellular resolution[2,3] and hundreds to potentially thousands of RNA species at single-cell resolution[4,5]. Mass spectrometry-assisted methods enable detection of the expression of a high number of proteins at the resolution of tissue patches[6,7] and tens of markers at subcellular resolution[8], and over hundred metabolites at cellular and subcellular resolutions[9,10]. Finally, barcoding-based approaches[11,12] facilitate the measurement of genome-wide expression at a resolution of hundreds of microns, i.e., several cells, and are being further developed to increase the resolution to below ten microns[13,14]. Complementally, we are also witnessing the rapid development of methods for spatial localization that combine limited amounts of spatially resolved data with richer, but dissociated single-cell data[15–18], which can alleviate the various shortcomings of the technologies. Therefore, there is a need for methods to analyse large amounts of rich and spatially-resolved data. These methods should ideally be able to handle the variety of produced data and scale well with future technology improvements.

Currently, there is a limited number of methods available for the analysis of high-resolution spatially-resolved data. One group of methods focuses on the analysis of the significant patterns and the variability of expression of individual markers[19–21] to describe the landscape of expression within a tissue. Another group of methods considers, more broadly, the analysis of the interactions between the markers within different spatial contexts, that is the expression in the directly neighboring cells or the effect of the expression of a marker in the

broader tissue structure. The methods within the latter group focus mainly on identifying interactions in the local cellular niche, by establishing the statistical significance of the distribution of automatically identified cell types in the neighborhood of each cell[22–24]. These methods assume a fixed form of nonlinear relationship between markers or have a predefined set of spatial contexts which can be explored. Spatial Variance Component Analysis (SVCA)[25], for example, goes a step further by examining intercellular interactions by decomposing the source of the variation to three fixed spatial contexts: intrinsic, environmental and intercellular effects.

We introduce here a Multiview Intercellular SpaTial modeling framework (MISTy), an explainable machine learning framework for knowledge extraction and analysis of single-cell, highly multiplexed, spatially resolved data. MISTy facilitates an in-depth understanding of marker interactions by profiling the intra- and intercellular relationships. MISTy is a flexible framework able to build models to describe the different spatial contexts, that is, the types of relationship among the observed expressions of the markers, such as intracellular regulation or paracrine regulation. For each of these contexts MISTy builds a component in the model, called a view. Furthermore, the views can also capture cell-type specific relationships, or focus on relations between different anatomical regions. Each MISTy view is considered as a potential source of variability in the measured marker expressions. Each view is then analyzed for its contribution to the total expression of each marker and is explained in terms of the interactions with other measurements that led to the observed contribution. Our approach is modular, easily parallelizable and thus scalable to samples with millions of cells and thousands of measured markers.

We validated MISTy on *in silico* data generated by a custom algorithm. We further applied our framework on an Imaging Mass Cytometry (IMC) dataset consisting of 46 breast cancer biopsies. We show that MISTy is able to extract and extend the set of inter-cellular interactions found with previous approaches. Finally, MISTy can extract knowledge about the interactions among signaling pathways and ligands expressed in the microenvironment from different spatial views. We demonstrate this on spatial transcriptomics data of breast cancer. These case studies illustrate the flexibility of MISTy to analyse diverse types of spatial omics data.

Results

MISTy: Multiview intercellular spatial modeling framework

MISTy is a late fusion multiview framework for the construction of a domain-specific, explainable model of the expression of markers (Figure 1). For each marker of interest in a sample, we can model cell-cell interactions coming from different spatial contexts as different views. The first and main view, containing all markers of interest, is the intrinsic view, where we relate the expression of other markers to a specific marker of interest within the same location. To capture the local cellular niche, we can create a view that relates the expression from the immediate neighborhood of a cell to the observed expression within that cell; we call this view a juxtaview. To capture the effect of the tissue structure, we can create a view that relates the expression of markers measured in cells within a radius around a given cell, and we call this view a paraview (see Methods).

Importantly, MISTy is not limited to the abovementioned views. Other views can be added to the pipeline that can offer an insight about relations coming not only as a function of space. For example, views can focus on interactions between different cell types, interactions within specific regions of interest within the sample or a higher level functional organization.

Formally, we consider a matrix $[Y]_{u,i}$ where each column represents a marker ($i = 1 \,..\, n$) and each row is a spatial location ($u = 1 \,..\, L$). $Y_{.,i}$ is the vector made by all observations of the marker i. MISTy models its expression as

$$Y_{.,i} = \alpha_I + \alpha_0 F_0(\tilde{Y}) + \sum_v \alpha_v (F_v(G_v(X, \tilde{Y}, T)), \qquad (1)$$

where $\tilde{Y} = Y_{.,\forall k \neq i}$, i.e. all markers except the target marker. F_v are models constructed by a machine learning algorithm (in this work we consider F to be Random Forests) for each view v. G are domain-specific functions that transform the data to generate informative variables (features) from the expression Y at the corresponding spatial localization X. Optionally, G can depend on other specific properties T, such as annotated functions, regions or cell-type. The G functions can be used to generate alternative views that can be inputs to the model function F. For example, given gene expression data, a function G can be used to infer pathway activities at each location. The corresponding variables can be input to MISTy to relate the activities of pathways at each location with

those from a broader spatial context. Finally, α are the late fusion parameters of the meta-model that balances the contribution of each view to the prediction.

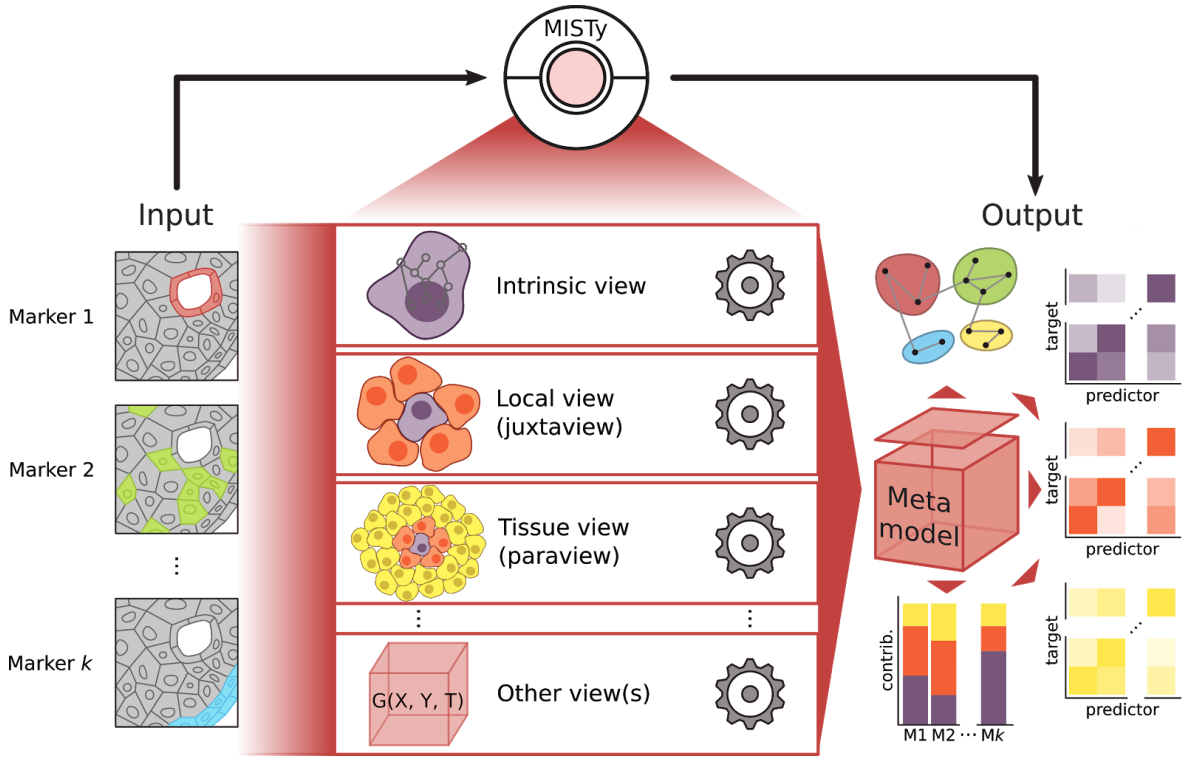

Figure 1. MISTy: An explainable multi-view framework for modeling intercellular interactions from highly multiplexed spatial data. *MISTy models marker relations coming from different spatial views: intrinsic, local niche view (juxtaview), the broader, tissue view (paraview), or others, based directly on marker expressions or derived typology or functional characterisations of the data. At output, MISTy extracts information about the contribution of different spatial views to the expression of markers in each cell. MISTy also estimates the markers' interactions coming from each view that explain those contributions. These results can be described qualitatively as communities of interacting markers for each view.*

The above model is trained in two steps. First, the models for each view are trained independently. MISTy models the intrinsic view $F_0(\tilde{Y})$ as a baseline view that is independent from the spatial localization of the cell. Other intercellular views are then added to $F_0(\tilde{Y})$. The user can add a number v of additional, intercellular views, and separately the effect of each view for each marker on the improvement in predictive performance of the multiview model. The contribution of each view is captured by the late fusion parameters α

of the meta-model. Second, we estimate α parameters of the meta-model after training the view-specific models independently, by linear regression.

In principle, MISTy can construct models for the functions F with any algorithm that fulfills two requirements. First, the algorithm should construct ensemble models, with constituents trained on a bootstrap sample (bag) from the data. Second, they should be or consist of explainable models. The first criteria guarantees the unbiased use of the measurements in both steps of model training. The predictions of the constituents of an ensemble model can be made on portions of the data (out-of-bag), that were not used for their training. The second criteria means that a global explanation of the model or the importances of the features can be obtained post-hoc from the trained models. As proof of principle, in this work we use Random Forests[26] for F, where the feature importances can be explained by the reduction of variance in the constituent trees.

MISTy generates a model for each marker of interest that can be readily used to make predictions of marker expressions under different conditions. For example, we can increase or reduce the expression of a certain marker *in silico* and explore the effects of the new condition. Importantly, we can use the model to estimate how much the different views, such as intrinsic or paracrine effects, contribute to the prediction of the expression of each target marker. At the first level, the meta-model can be interpreted in two different ways. First, to answer the question of how much the intercellular views improve the prediction of the expression in addition to the intracellular view. This can be achieved by comparing the predictive performance of a single intracellular view vs all views combined in a meta-model. Second, by comparing the values of the fusion parameters, we can investigate how much the individual views contribute to explaining the marker expression that led to the aforementioned improvement in predictive performance.

Given this information, at a second level, we can further analyse the feature importances. For each target marker, we can inspect each view-specific model and analyse how important is the contribution of each marker in that view to the prediction of the expression of the target marker. These importances correspond to potential relations between the predictor and the target marker in the specific spatial or other context modelled by the corresponding view. MISTy outputs the estimated importances of significant marker relations. Since these relations are based on the importance of a marker in predicting the target they cannot be assumed to be directly causal nor directional. The relations between markers may occur

through a network of intermediate interactions in the specific biological context, which can be further explored by enrichment of these relations using curated databases of intra- and intercellular interactions.

Finally, if multiple samples are available during the analysis, the relations from individual samples are aggregated to produce robust results (see Methods). By aggregation, we accentuate consistently inferred interactions from individual samples and reduce the number of false positive interactions.

In silico performance

We first assessed the performance of MISTy to reconstruct *in silico* intra- and intercellular interaction networks. For this, we created a tissue simulator that can mimic the interactions of different cell-types through ligand binding and subsequent signaling events (Figure 2A; see Methods). The dynamic model simulates the production, diffusion, degradation and interactions of 11 molecular species until a steady state distribution of markers are reached. The simulated values for every molecular species, at every location is recorded and passed as input to MISTy (Supp Figure 1). Information about the different cell-types, their intracellular wiring or which cell type expresses which ligand is not given as input to MISTy. We use this procedure to estimate the robustness of MISTy to infer interactions.

The MISTy pipeline for *in silico* data consists of two views, intracellular view and broader tissue structure view (paraview). When we compare the predictive performance of this model to a model with a single intrinsic view, we see the highest improvement in predictive performance, for the expression of markers ligC, ligB, ligA and ECM, which are the diffusing molecules in the model. The improvement is reflected in the observed contributions of the tissue structure view (Figure 2B).

We evaluated the performance of MISTy to recover interactions among markers. MISTy identified strong importance between prodC-ligC and also between ECM-protE (Figure 2C). These two steps are part of the ECM production pathway involving cellType2 and cellType3. In the dynamical model, prodC produces ligC in cellType2, which diffuses on the lattice and activates protE in both cellType1 and cellType3. In turn, protE activates ECM production in cellType3. Note that these interactions appear both in the intrinsic and paraview views. This is because these interactions involve diffusive compounds (ligC and ECM), that are produced by intracellular proteins and then diffuse to the neighbourhood.

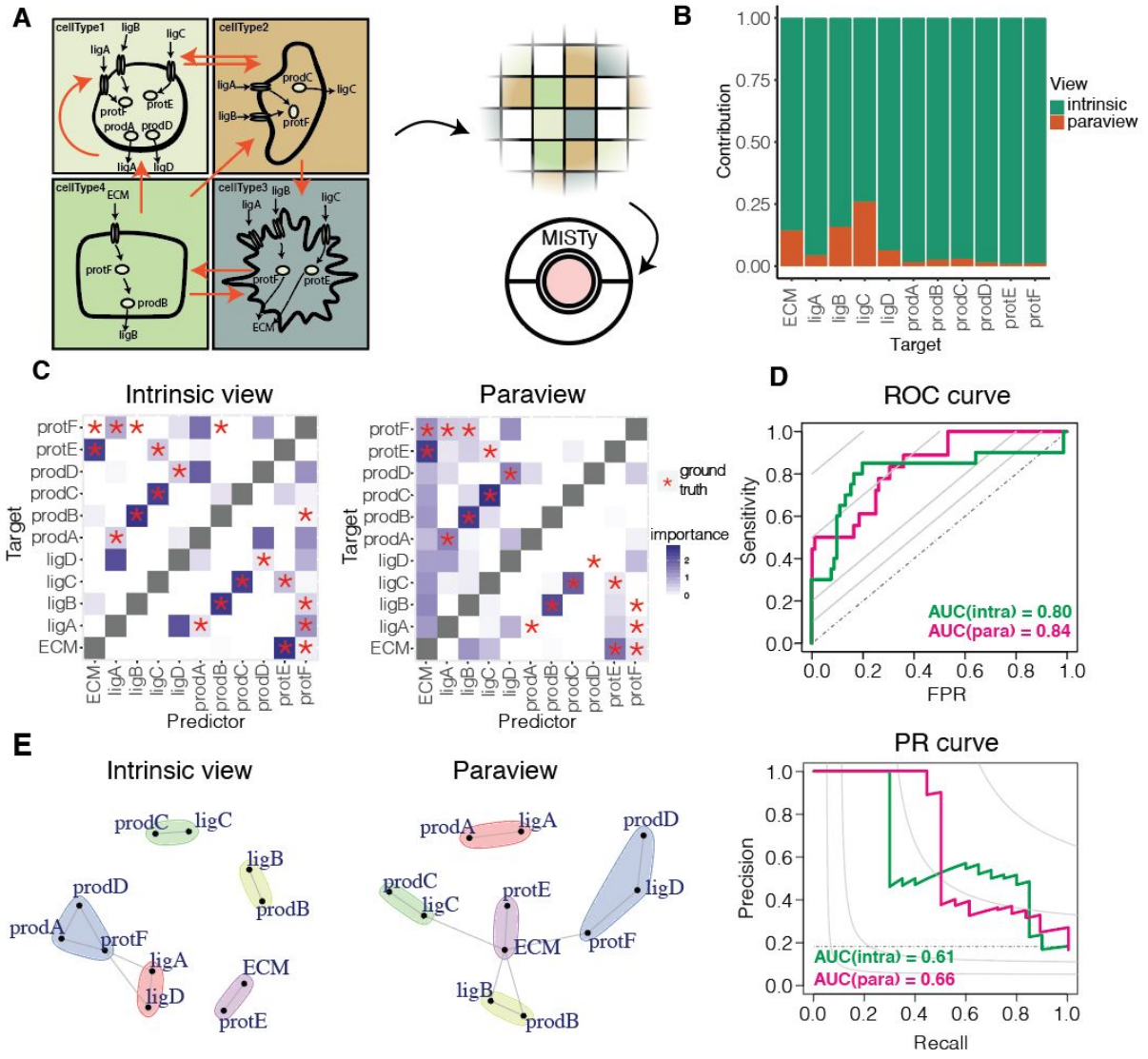

Figure 2. Evaluating MISTy on in silico data. *(A) MISTy was evaluated on the task of reconstruction of simulated interaction networks. Models of intra- (black arrows) and intercellular (orange arrows) interactions of four different cell types, arranged on a grid representing a tissue, were used to simulate measurements of 11 molecular species. (B) Contribution of each view to the prediction of the marker expressions in the meta-model. The stacked barplot represents normalized values of the fusion coefficients of the respective views for each marker. (C) Marker interactions in the intrinsic and paraview. Heatplot shows the interactions found by MISTy, red stars highlight the ground truth interactions. (D) Receiver operating characteristic (ROC) and precision-recall (PR) curves depicting the aggregate performance of MISTy on all ten samples for the intrinsic view and paraview. The dashed lines represent the expected performance of an uninformed classifier, the gray iso-lines represent points in ROC space with informedness (Youden's J statistic) equal to 0.1, 0.2, 0.5 and 0.8 and points in PR space with F1 measure equal to 0.1, 0.2, 0.5 and 0.8. (E) Communities of marker interactions identified by the Louvain method for community detection on the heatplots.*

The production of ligB, ligC and ECM by the respective prodB, prodC and protE nodes are clearly captured (Figure 2C, 2E). There is also a strong interaction reported between ligA and ligD, as well as between prodA and prodD in the intrinsic view. In the model, there is no connection between these nodes. Therefore, they are considered as false positives. However, we can notice that all of them are co-expressed in cellType1, which can explain the result.

Across the individual samples, we observed variance in MISTy's performance, in both the area under the receiver operating characteristic curve (AUROC) and the area under the precision-recall curve (AUPRC) (Supp Figure 2). We aggregated the results from all layouts (see Methods section for details) and calculated the performance (Figure 2D). The aggregation strategy maximized the extracted knowledge available in the samples (AUROC= 0.80 and 0.84 and AUPRC = 0.61 and 0.66 for the intrinsic and the paraview, respectively). In summary, MISTy is able to reliably extract interactions in the *in silico* case study.

Application to an Imaging Mass Cytometry breast cancer dataset

We applied MISTy on an Imaging Mass Cytometry dataset consisting of 46 samples of breast cancer representing all three grades coming from 26 patients[24]. We processed each sample with MISTy independently and we aggregated the outputs in four ways: for each of the three tumor grades separately, and for all samples. We designed the MISTy pipeline for this task to include three different views: An intrinsic view, a view focusing on the local celular niche (juxtaview), and a view capturing the effect of the broader tissue structure (paraview), as illustrated in Figure 2B and detailed in the Methods section.

In the aggregated results from all samples, we found that the multiview model resulted in significant improvements in variance explained of up to 25% over using the intrinsic view only. This is consistent with results obtained with another method, SVCA, on the same data[25] (Supp Figure 3). Highest median improvement was detected for the markers pS6 (median 2.2%, max 17.7%), SMA (median 3.6%, max 10%) and Ki67 (median 1.8%, max 7.9%). This is expected, since these three markers have distinct spatial distributions: pS6 represents "active" stroma present in distinct regions of the tumor microenvironment, SMA represents smooth muscle Actin, which is expressed in ductal structures and blood vessels; and Ki67 is a marker of proliferation and is highly expressed in tumor regions. The highest change in variance explained (24.9%) in a single sample was observed for CAIX, a marker of hypoxia. In grade 1 tumor samples (n = 16), we observed the highest improvement for markers

Cytokeratin7 (median 5.6%, max 14%) and signaling marker pErk12 (median 1.6%, max 20.4%) (Supp Figure 4A). In grade 2 tumor samples (n = 3), we observed the highest improvement in CD3 (median 1.1%, max 18.4%) and Slug (median 1%, max 19%) (Supp Figure 4B). In grade 3 samples (n = 24) we observed the highest improvement for CAIX (median 0.6%, max 23.5%) and pS6 (median 6.2%, max 19.5%) (Supp Figure 4C). This was expected due to higher levels of hypoxia at an advanced tumor stage. In addition, pS6 was shown to interact with CAIX, which explains the coupled appearance. The results illustrate how MISTy can recapitulate previous findings without the need of single cell clustering and cell type annotation using prior-knowledge[24].

We next analyzed the contribution of each view to the prediction of the multi-view model (Figure 3A). Across all aggregations of the samples, a high contribution of the juxtaview was observed for immune cell markers CD20, CD3, CD44, and CD68 (mean contribution to prediction of 18%). This finding is consistent with the results obtained with SVCA[25], where it was shown that the highest increase in variance explained is due to cell-cell interactions, which in turn were found to be significantly correlated with the average number of neighbors per cell. With MISTy we further dissected the effect of the juxtaview and paraview. We find that a significant contribution (higher value of the fusion parameter in the meta-model) comes from the paraview compared to the juxtaview. This is consistent with the increase in variance explained in the samples. Namely, the mean contribution to the prediction of the intrinsic view was 69%, of the juxtaview 9% and of the paraview 22%.

To explain the contributions of each view, we further analyzed the importances of the features as predictors for the expression of each marker of interest (Figure 3B, C and D). In the intrinsic view, we observed groups of markers (communities) that consistently interact in grade-specific analyses and across all samples (Figure 3E). In the juxtaview we observed a community of interactions involving epithelial markers (Cytokeratin 7, Cytokeratin 8/18 and E-cadherin) on one hand, and community of interactions involving stromal markers (SMA, Fibronectin and Vimentin) on the other. There is a pronounced decline in the number of highly important features in the juxtaview and the paraview, when comparing grade 1 and grade 3 tumors (Supp Figures 5, 6 and 7). This is likely due to cells being mainly intrinsically driven in grade 3 samples, due to high density and advanced state of cancer. In other words, normal tissues are highly structured, and the underlying tissue structure is critical to perform tissue relevant functions. A tumor destroys the underlying structure and creates a more “random” distribution of tumor / stromal cells.

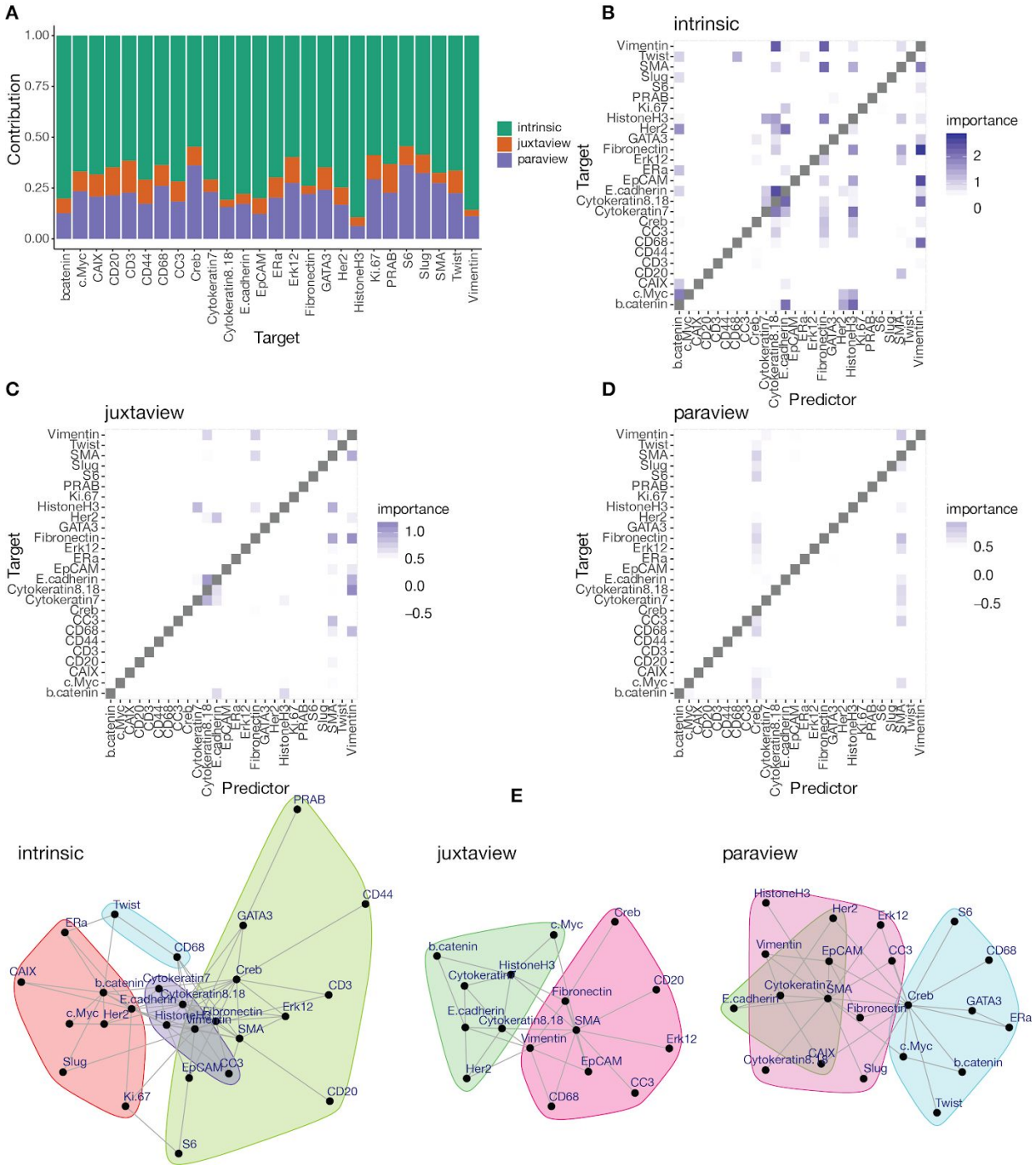

Figure 3. Application of MISTy to the Imaging Mass Cytometry dataset. *(A) Normalized values of the fusion coefficients of the respective views for each marker. (B) Importances of marker expression as predictors of the expression of each target marker in the intrinsic view. (C) Importances in the juxtaview. (D) Importances in the paraview. The importances are extracted from the view-specific models for each target marker. (E) Communities of marker interactions identified by applying the Louvain method for community detection on the symmetric adjacency matrices generated from the heatplots.*

Application to a spatial transcriptomics breast cancer dataset

An important feature of MISTy is its independence from the technology and flexibility to analyze different spatially-resolved data. Even more, the properties of the data obtained from different technologies can be leveraged to create different explanatory views.

To illustrate this, we analyzed the spatial gene expression profiles of two sections of a sample of invasive ductal carcinoma in breast tissue profiled with 10x Visium[27]. The 10x Visium slides contain 4992 total spots of 55 μm in diameter per captured area that enable the profiling of up to 10 cells per spot. With this technology, thousands of spatially resolved genes can be profiled simultaneously within a sample, allowing for characterization of molecular processes.

Previously, we have shown the utility of the footprint-based method PROGENy to robustly estimate the activity of signaling pathways, in both bulk and single-cell transcriptomics[28,29]. PROGENy estimates the pathways' activity by looking at the expression changes in downstream target genes, rather than on the genes that constitute the pathway itself. Due to the resolution and the gene coverage of 10x Visium slides, the same approach can be applied to spatial transcriptomics datasets to enhance the functional view of the data. We estimated pathway activities for two reasons: 1) to reduce the dimensions of the data into interpretable and functionally relevant features, while still using the information of as many genes as possible, and 2) to provide a set of features that are more stable than the sparse expression of marker genes.

For each sample section, we estimated the activities of 14 cancer relevant signaling pathways of each spot using PROGENy[28] (Figure 4A). We observed clear localized activities of all pathways (Supp Figures 8 and 9). While crosstalk mechanisms are expected within a spot, we hypothesized that the local pathway activity can also be regulated by neighbouring cells in other spots via direct ligand-receptor interactions or indirect processes triggered by the microenvironment. Therefore, we identified a set of 275 expressed genes in both sections annotated as ligands (Figure 4A) in the meta-resource OmniPath[30] (see Methods) and designed the MISTy pipeline to model pathway activities using three different views: An intrinsic view of pathway activities and two functional paraviews focusing on pathway activity and ligand expression, respectively (see Methods).

The multiview model improved the variance explained by up to 11% compared to the single, intrinsic view (Supp Figure 10). We found a mean contribution of 74% of the intrinsic view, 16% of the ligand expression paraview and 10% of the pathway activity paraview to the prediction of pathway activities in the multi-view model (Figure 4B).

The ligand expression paraview contributed the most to the prediction of the Estrogen and Hypoxia pathways. These pathways also showed the highest average improvement in variance explained with the multiview model. The moderate contribution of the functional paraviews could be due to the pathway crosstalk within a spot. The importances of the features used as predictors in each view are consistent with biological processes. In the intrinsic view, we observed relationships between NFkB and TNFa, and P53 and MAPK that have been reported previously[28]. To illustrate this, we can look at the spatial distribution of P53 and MAPK activity and observe their anticorrelation (Figure 4C). Additionally, when compared with the importances of the pathways in the paraview, we found similar interactions suggesting consistency of function in large areas of the tissue. Moreover, we also observed new interactions among pathways that may represent long distance dependencies. For example JAK-STAT as a predictor of WNT, an interaction that is not present in the intrinsic view (Figure 4D). Among the top interactions observed between the pathway activities and ligands (Figure 4E), we recovered the relationship between SEMA4C and Estrogen that has been linked to poor disease outcome in luminal type breast cancers[31]. SEMA4B is an important predictor of Hypoxia that is in concordance with the known repression of this protein with HIF1-a (Figure 4E)[32,33]. TGFb has a strong interaction with extracellular matrix proteins such as VCAN, COL5A1, and COL16A1. This effect is in agreement with the reported regulation of this pathway to proteins responsible for the collagen remodeling in other cancers[34,35]. Together, these results show the effectiveness of MISTy in retrieving tissue-level interactions between different functional layers of information.

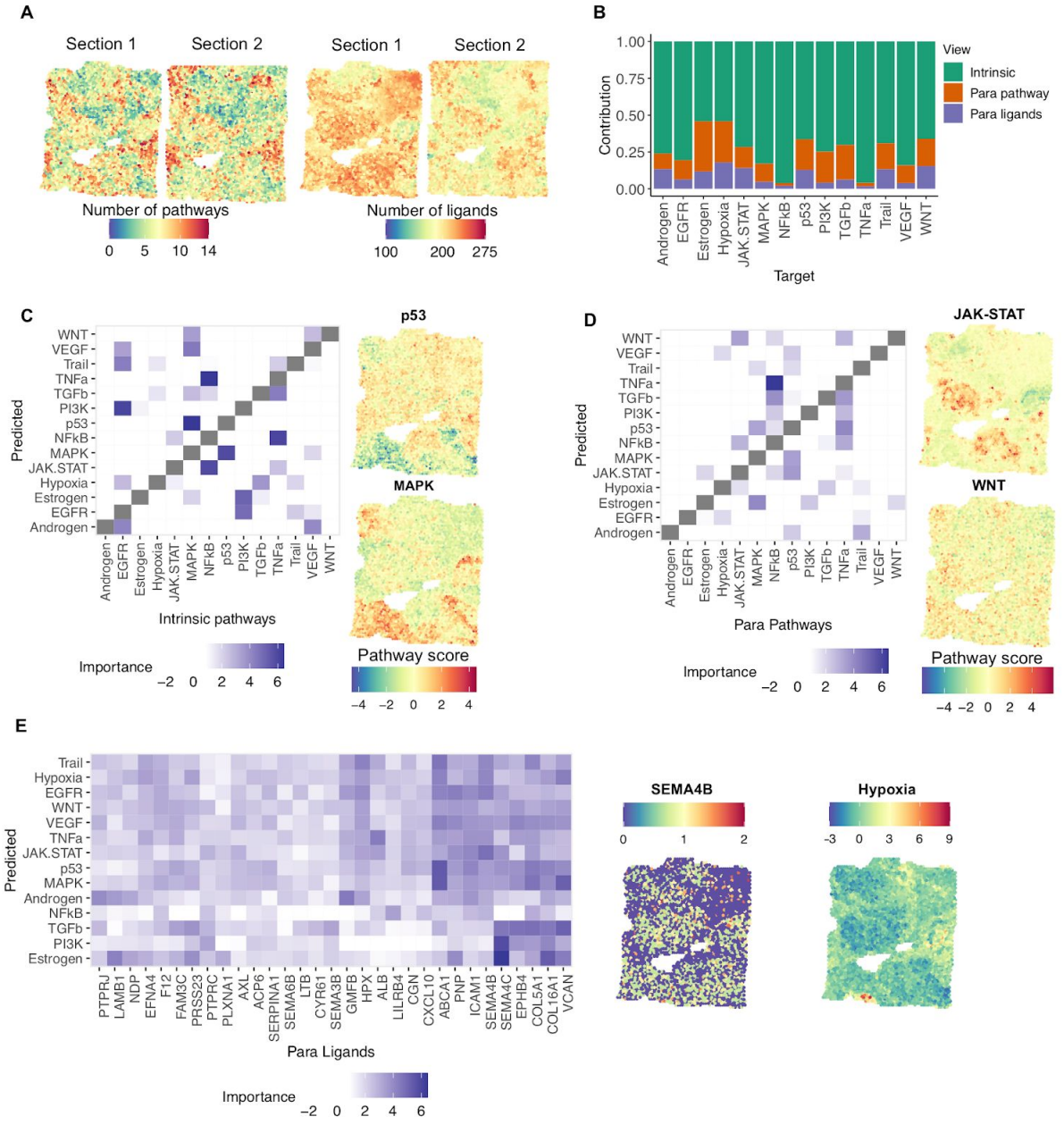

Figure 4. Application of MISTy to a spatial transcriptomics dataset. *(A) Pathway activities and ligand expression coverage in the two sections analyzed. (B) Contribution of each view to the prediction of the pathway activities in the meta-model. The stacked barplot represents normalized values of the fusion coefficients of the respective views for each pathway. (C) Variable importances for the intrinsic view; pathway activity scores of p53 and MAPK in the first section. (D) Variable importances for the pathway paraview; pathway activity scores of JAK-STAT and WNT in the first section. (E) Top variable importances for the ligands paraview (mean importance > 2); expression of SEMA4B and pathway activity score of Hypoxia in the first section.*

Discussion

Here we present MISTy, an explainable framework for the analysis of highly multiplexed spatial data. It can scale to match the increasing complexity and resolution of data due to recent and upcoming technological advancements. MISTy complements the methods that leverage spatial information to explore intercellular interactions. The current approaches mainly focus only on the local cellular niche, i.e., the expressions measured in the immediate neighborhood of each cell[22–24]. Other methods that consider the broader tissue structure are relatively inflexible[25]. They consider a fixed form of nonlinear relationship between markers at predefined spatial contexts, and they do not scale well due to their high computational complexity. In contrast, MISTy offers a flexible range of spatial analyses in a scalable framework. We present a selected set of pipelines for the analysis of spatial data, using not only the marker expressions but also derived features, such as pathway activities.

We established a performance baseline for MISTy on *in silico* data before applying MISTy to real-world data. We showed that MISTy achieves high performance on the task of reconstructing the intra- and inter-cellular networks of interactions.

We then applied MISTy to two real-world spatial-omics data sets from breast cancer samples. First, we applied MISTy on imaging mass cytometry data, capturing dozens of protein markers at (sub)cellular resolution. The results show that we were not only able to recapitulate results from the literature without prior-knowledge-based cell type annotation, but to also generate new hypotheses. Our results show that the information that is available from the expression of markers in the broader tissue structure is often more important than their expression in the local cellular niche. This highlights that not only cellular niches but also tissue structure have a direct impact on cellular states and should be included into the “microenvironment” definition.

Further, we applied MISTy on a spatial transcriptomics data set, one of the first publicly available samples measured with 10x Visium. Here, thousands of transcripts are measured in spots containing several cells. Given the richness of the data, we were able to go a step further and consider the analysis of functional features, in the form of pathway activities which were inferred from the data. In particular, we showed the crosstalk between pathways and the ligand-pathway interactions in the context of the broader tissue structure in breast cancer.

Although the interactions extracted by MISTy cannot be considered directly as causal, they can facilitate the downstream analysis of biological systems at the tissue level in several directions: (i) To predict the behavior of systems under perturbations, by using the MISTy model to generate marker expressions based on the new conditions; (ii) To guide the reconstruction of multicellular causal signaling networks, using databases to identify mechanisms giving rise to the extracted interactions; and subsequently (iii) To construct mechanistic models of the dynamical behavior of the system constrained by the extracted explanations.

The work we presented lays the foundation for further exploration of MISTy in several directions. One direction is to address the scalability of MISTy to millions of cells and thousands of markers per sample, which is beyond what the available technologies can offer, but is likely to come in the near future. To do this we are exploring approximate but accurate methods to replace the computationally expensive step of generating views where the pairwise distances between all cells need to be calculated. Another direction is the exploration of the performance that can be achieved by MISTy with different ensemble approaches using various types of explainable constituent models. Finally, MISTy can be used to generate more specific views. In particular, views that capture the spatial expression of specific cell types, so that we can dissect the spatial interactions between different cell types, or views that focus on regions of the tissue, for example, healthy vs pathological, where we would model the interactions between the functionally different regions.

In summary, we believe that MISTy is a valuable tool to analyse spatially resolved data, adaptable to multiple data modalities and biological contexts, that will also evolve as experimental techniques improve. MISTy is freely available as an open-source R package.

Methods

In silico benchmark

The *in silico* model is a two-dimensional cellular automata model that focuses on signaling events, therefore cell growth, division, motility and death are neglected. First, we created ten random layouts. To account for cellular heterogeneity in the tissue, we assigned one of four different cell-types $CT1, ...CT4$, to each spot of the layout or left it empty (intercellular

space). Each of these cell-types has a distinct set of receptors expressed and distinct intracellular wiring. To keep the model simple, we considered 11 biological species S = {ligands: ligA, ligB, ligC and ligD; intracellular proteins: protE, protF; ligand producing nodes: prodA, prodB, prodC and prodD}. The intracellular processes involve two layers, first the ligand activation of signaling hubs, represented by protE and protF, and ligand production/secretion regulated by proteins (prodA, prodB, probC and prodD)(Figure 2A). The model simulates the production, diffusion, degradation and interactions of these 11 molecular species on a 100-by-100 grid. Ligands are produced in each cell-type based on the activity level of their production nodes and then freely diffuse, degrade or interact with other cells on the grid. Other molecular species involved in signaling are localised in the intracellular space and their activity depends on ligand binding and intracellular wiring.

The model is formally stated by the following partial differential equations for each species:

$$\frac{\partial c_s(x,y,t)}{\partial t} = d_s \Delta c_s(x,y,t) + P_s(x,y,t) - D_s(x,y,t) \quad . (2)$$

This equation describes the diffusion, the production/activation and the degradation of the species. We made the following assumptions. $c_s(x,y,t)$ is the concentration of species $s \in S$ at the grid point (x,y) at time t. The diffusion is homogenous across the image, the diffusion coefficient of species *s* is d_s. Only ligands and ECM are diffusing, other intracellular molecules cannot leave the cell.

The production term includes the generation of ligands and the activation of intracellular proteins. It depends on the cell-types and the activity of the production node: for ligands, *ligX* production depends on *prodX* node: $P_i(x,y,t) = \alpha_{i,ct} prodX_i(x,y,t)$ for $i \in \{ligA, ligB, ligC, ligD\}$ and $ct \in CT$, the $\alpha_{i,ct}$ coefficient defines which cell type produces which proteins and how strongly the production depends on the activity of the production node.

For intracellular proteins, the protein activity depends on the abundance of the ligands that activate its pathway: $P_i(x,y,t) = \beta_{i,l}^{ct} c_l(x,y,t)$, for $i \in \{protE, protF\}$ and $l \in \{ligA, ligB, ligC, ligD\}$. The $\beta_{i,l}^{ct}$ encodes the interactions between the ligand and the proteins in each cell type as shown in the graph in Figure 2.

Degradation is proportional to the concentration of ligands, intracellular proteins and ECM, $D_s(x,y,t) = \gamma_s c_s(x,y,t)$, where γ_s is a constant degradation coefficient.

The above model was simulated from a randomised initial condition until a steady state distribution of the species and activity was achieved (Supp Figure 1).

We aggregated the interactions from the mechanistic model for the different cell types in joint binary matrices of directed ground truth interactions for the different views. To compare the matrices to the importance matrices from the output of MISTy, we transformed the joint matrices into undirected matrices $A_u = sgn(A + A^T)$. We then quantified the performance of MISTy for the task of reconstruction of intra- and intercellular networks from the true and the extracted interaction matrices.

Data acquisition and processing

Imaging Mass Cytometry

The Imaging Mass Cytometry dataset consists of 46 samples from 26 breast cancer patients with varying disease grades[24]. The raw data was segmented and single cell features were extracted with histoCAT. The samples contain between 267 and 1455 cells with measured expression of 26 proteins / protein modifications. The cell-level data was preprocessed as defined in Arnol et al.[25] in order to assure the validity of direct comparison of results.

Spatial transcriptomics

The data and sample information were obtained from 10x Genomics[27]. The data consists of spatial transcriptomic measurements of two sections of a sample analyzed with 10x Genomics Visium. The sections come from tissue from a patient with grade 2 ER^+, PR^-, $HER2^+$, annotated with ductal carcinoma in-situ, lobular carcinoma in-situ and invasive carcinoma. The mean sequencing depths were reported to be 149,800 and 137,262 reads per spot for a total of 3,813 and 4,015 spots per section respectively. The median UMI counts per spot were reported as 17,531 and 16,501, and the median genes per spot as 5,394 and 5,100 respectively. The raw data was preprocessed and count matrices were generated with *spaceranger-1.0.0*. Individual count matrices were normalized with *sctransform* implemented in Seurat 3.1.2[36]. For each spot, we estimated signaling pathway activities with PROGENy's model matrix using the top 1000 genes of each transcriptional footprint. We retrieved from Omnipath[30] all proteins labeled as ligands and in each dataset we filtered all ligands whose expression was captured in at least 30% of the spots.

View generation

For the application of MISTy on IMC and spatial transcriptomics data, in addition to the intrinsic view, we considered creating views by aggregating the available spatial and expression information in two ways. For the IMC data we created a view that describes the local cellular niche (juxtaview) and a view that describes the broader tissue structure (paraview), both created using the measured marker expression directly. For the spatial transcriptomics data we created a paraview using the estimated pathway activities at each patch and a paraview using the measured expressions of a set of ligands.

We consider a dataset $D = [X_{(n\times s)}\ Y_{(n\times k)}]$, represented as a matrix of dimensions $n \times (s+k)$ of spatially-resolved highly-multiplexed measurements of a sample, where n is the number of measured units (pixels, cells, patches) available in the sample, s is the number of spatial dimensions in the geometry matrix X and k is the number of measured markers in the expression matrix Y.

The juxtaview was generated by summing the expressions of its direct neighboring cells, i.e., $G_c = \sum_{j \in N_c} \tilde{Y}_{j,\cdot}$, where N_c represents the set of neighboring cells of cell c. The neighboring cells for each cell can be determined either during image segmentation, for example by setting a threshold of membrane to membrane distance, or, as in the case for the application of MISTy on IMC data, by post-hoc neighborhood estimation. For the application of MISTy on IMC data the neighborhood of each cell in a sample was estimated by constructing a cell graph by 2D Delaunay triangulation followed by removal of edges with length larger than the 25th percentile of all pairwise cell distances across all samples, which corresponded to 11.236 microns from the cell centroid.

The paraview was generated by weighted aggregation of the expressions of all cells (patches) from the sample $G_c = \sum_{j=1}^{n} e^{-d_{ij}^2/l^2} \tilde{Y}_{j,\cdot}$, where d_{ij} is the Euclidean distance between cells i and j, calculated from matrix X and l is a parameter controlling the shape of the weighting radial basis function. The parameter l corresponds to the radius around the cell where we consider the values of the weighting function to allow for substantial contribution of the measured expressions. For the application of MISTy to both IMC and spatial

transcriptomics data, we optimized the value for the parameter l. For each sample, we constructed models for each marker, with parameter $l \in \{2, 5, 10, 20, 50, 100\}$. This corresponds to an effective radius of influence of 2 to 100 pixels or micrometers. Then, for each marker we selected the value for l such that the estimated improvement in predictive performance by using the multi-view model in contrast to the intrinsic view model is maximized. For each model (Random Forest), we estimate the predictive performance by measuring the variance explained on out-of-bag samples.

Importance weighting and result aggregation

To calculate the interaction importances from a sample we used information from the two layers of interpretability and explainability: the values of the fusion parameters (α_v in Eq. (1)) in the meta-model and their respective p-values $p_k^{(v)}$ for each target marker k and the importances $I_{kj}^{(v)}$ of features j for the prediction of each target marker extracted from the predictive model for view v yields the MISTy interaction importance:

$$M_{kj}^{(v)} = \frac{I_{kj}^{(v)} - \bar{I}_k^{(v)}}{\sigma_{I_k^{(v)}}^2}(1 - p_k^{(v)}) \qquad (3).$$

Since the importances $I_{kj}^{(v)}$ extracted from a Random Forest model (used for the current instance of MISTy) represent the amount of variance reduction in the target expression, the MISTy interaction importances correspond to the standardized value (by mean $\bar{I}_{kj}^{(v)}$ and variance $\sigma_{I_k^{(v)}}^2$) of the variance reduction weighted by the quantile $1 - p_k^{(v)}$ of the statistic under the null hypothesis of zero contribution of the fusion coefficient for view v for target k in the linear meta-model. The importance derived from variance reduction can be generalized to any measure of impurity or values extracted by other feature importance estimation methods, given the model constituents of MISTy. Since the MISTy importances are standardized, importances from multiple samples can then be aggregated by simple averaging, while their interpretation remains the same.

For views that contain the same set of predictors as targets, we also identified the communities of interactions from the estimated importances. For this, we transformed the square matrix A of estimated predictor-target interactions to an undirected graph adjacency matrix as $A_p = A + A^T$. We then extract the community structure from the graph using the

Louvain algorithm[37], a commonly used algorithm for community detection by grouping nodes, such that the modularity of the graph is maximized.

Code availability

The code of MISTy as an R-package as well as the scripts to generate the results shown in this paper are available at https://saezlab.github.io/misty/.

Acknowledgements

JT acknowledges the financial support from the European Union and the Slovenian Ministry of Education, Science and Sport (agreement No. C3330-17-529021). DS was supported by an Early Postdoc Mobility fellowship (no. P2ZHP3_181475). We would like to thank Nicolàs Palacio-Escat for the Figure 1 design and Olga Ivanova for providing feedback on the manuscript.

Author contributions

JT designed and implemented MISTy. JT and JSR designed the experimental evaluation. JT implemented the pipelines for the analysis of the data with MISTy. AG designed and implemented the cellular automata model and generated the *in silico* data and analysed the results. RORF generated the functional views of the spatial transcriptomics data and analysed the results. DS analysed the results of the IMC and ST breast cancer data. JSR supervised the project. JT drafted the manuscript. All authors contributed to the manuscript writing. All authors read, commented, and approved the final manuscript.

References

1. Chen, X., Teichmann, S. A. & Meyer, K. B. From Tissues to Cell Types and Back: Single-Cell Gene Expression Analysis of Tissue Architecture. *Annual Review of Biomedical Data Science* vol. 1 29–51 (2018).
2. Gut, G., Herrmann, M. D. & Pelkmans, L. Multiplexed protein maps link subcellular organization to cellular states. *Science* **361**, (2018).
3. Lin, J.-R. *et al.* Highly multiplexed immunofluorescence imaging of human tissues and tumors using t-CyCIF and conventional optical microscopes. *Elife* **7**, (2018).
4. Chen, K. H., Boettiger, A. N., Moffitt, J. R., Wang, S. & Zhuang, X. RNA imaging. Spatially resolved, highly multiplexed RNA profiling in single cells. *Science* **348**,

aaa6090 (2015).

5. Lubeck, E., Coskun, A. F., Zhiyentayev, T., Ahmad, M. & Cai, L. Single-cell in situ RNA profiling by sequential hybridization. *Nature methods* vol. 11 360–361 (2014).
6. Aichler, M. & Walch, A. MALDI Imaging mass spectrometry: current frontiers and perspectives in pathology research and practice. *Lab. Invest.* **95**, 422–431 (2015).
7. Butler, H. J. *et al.* Using Raman spectroscopy to characterize biological materials. *Nature Protocols* vol. 11 664–687 (2016).
8. Giesen, C. *et al.* Highly multiplexed imaging of tumor tissues with subcellular resolution by mass cytometry. *Nat. Methods* **11**, 417–422 (2014).
9. Rappez, L. *et al.* Spatial single-cell profiling of intracellular metabolomes in situ. *bioRxiv* 510222 (2019) doi:10.1101/510222.
10. Passarelli, M. K. *et al.* The 3D OrbiSIMS—label-free metabolic imaging with subcellular lateral resolution and high mass-resolving power. *Nature Methods* vol. 14 1175–1183 (2017).
11. Rodriques, S. G. *et al.* Slide-seq: A scalable technology for measuring genome-wide expression at high spatial resolution. *Science* **363**, 1463–1467 (2019).
12. Ståhl, P. L. *et al.* Visualization and analysis of gene expression in tissue sections by spatial transcriptomics. *Science* **353**, 78–82 (2016).
13. Vickovic, S. *et al.* High-definition spatial transcriptomics for in situ tissue profiling. *Nat. Methods* **16**, 987–990 (2019).
14. Stickels, R. R. *et al.* Sensitive spatial genome wide expression profiling at cellular resolution. *bioRxiv* 2020.03.12.989806 (2020) doi:10.1101/2020.03.12.989806.
15. Bageritz, J. *et al.* Gene expression atlas of a developing tissue by single cell expression correlation analysis. *Nature Methods* vol. 16 750–756 (2019).
16. Nitzan, M., Karaiskos, N., Friedman, N. & Rajewsky, N. Gene expression cartography. *Nature* **576**, 132–137 (2019).
17. Stuart, T. *et al.* Comprehensive Integration of Single-Cell Data. *Cell* **177**, 1888–1902.e21 (2019).
18. Tanevski, J. *et al.* Predicting cellular position in the Drosophila embryo from Single-Cell Transcriptomics data. *bioRxiv* (2019).
19. Sun, S., Zhu, J. & Zhou, X. Statistical analysis of spatial expression patterns for spatially resolved transcriptomic studies. *Nat. Methods* **348**, aaa6090 (2020).
20. Edsgärd, D., Johnsson, P. & Sandberg, R. Identification of spatial expression trends in single-cell gene expression data. *Nat. Methods* **15**, 339–342 (2018).
21. Svensson, V., Teichmann, S. A. & Stegle, O. SpatialDE: identification of spatially

variable genes. *Nat. Methods* **15**, 343–346 (2018).

22. Keren, L. *et al.* A Structured Tumor-Immune Microenvironment in Triple Negative Breast Cancer Revealed by Multiplexed Ion Beam Imaging. *Cell* **174**, 1373–1387.e19 (2018).
23. Goltsev, Y. *et al.* Deep Profiling of Mouse Splenic Architecture with CODEX Multiplexed Imaging. *Cell* **174**, 968–981.e15 (2018).
24. Schapiro, D. *et al.* histoCAT: analysis of cell phenotypes and interactions in multiplex image cytometry data. *Nat. Methods* **14**, 873–876 (2017).
25. Arnol, D., Schapiro, D., Bodenmiller, B., Saez-Rodriguez, J. & Stegle, O. Modeling Cell-Cell Interactions from Spatial Molecular Data with Spatial Variance Component Analysis. *Cell Rep.* **29**, 202–211.e6 (2019).
26. Breiman, L. Random Forests. *Mach. Learn.* **45**, 5–32 (2001).
27. Datasets -Spatial Gene Expression -Official 10x Genomics Support. https://support.10xgenomics.com/spatial-gene-expression/datasets.
28. Schubert, M. *et al.* Perturbation-response genes reveal signaling footprints in cancer gene expression. *Nat. Commun.* **9**, 20 (2018).
29. Holland, C. H. *et al.* Robustness and applicability of transcription factor and pathway analysis tools on single-cell RNA-seq data. *Genome Biol.* **21**, 36 (2020).
30. Türei, D., Korcsmáros, T. & Saez-Rodriguez, J. OmniPath: guidelines and gateway for literature-curated signaling pathway resources. *Nat. Methods* **13**, 966–967 (2016).
31. Gurrapu, S., Pupo, E., Franzolin, G., Lanzetti, L. & Tamagnone, L. Sema4C/PlexinB2 signaling controls breast cancer cell growth, hormonal dependence and tumorigenic potential. *Cell Death Differ.* **25**, 1259 (2018).
32. pubmeddev & Jian H, E. al. Hypoxia and hypoxia-inducible factor 1 repress SEMA4B expression to promote non-small cell lung cancer invasion. - PubMed - NCBI. https://www.ncbi.nlm.nih.gov/pubmed/24474252.
33. Jian, H., Liu, B. & Zhang, J. Hypoxia and hypoxia-inducible factor 1 repress SEMA4B expression to promote non-small cell lung cancer invasion. *Tumour Biol.* **35**, 4949–4955 (2014).
34. Cheon, D.-J. *et al.* A collagen-remodeling gene signature regulated by TGF-β signaling is associated with metastasis and poor survival in serous ovarian cancer. *Clin. Cancer Res.* **20**, 711–723 (2014).
35. Yeung, T.-L. *et al.* TGF-β modulates ovarian cancer invasion by upregulating CAF-derived versican in the tumor microenvironment. *Cancer Res.* **73**, 5016–5028 (2013).
36. Hafemeister, C. & Satija, R. Normalization and variance stabilization of single-cell

RNA-seq data using regularized negative binomial regression. *Genome Biol.* **20**, 1–15 (2019).

37. Blondel, V. D., Guillaume, J.-L., Lambiotte, R. & Lefebvre, E. Fast unfolding of communities in large networks. *Journal of Statistical Mechanics: Theory and Experiment* vol. 2008 P10008 (2008).

Supplementary figures

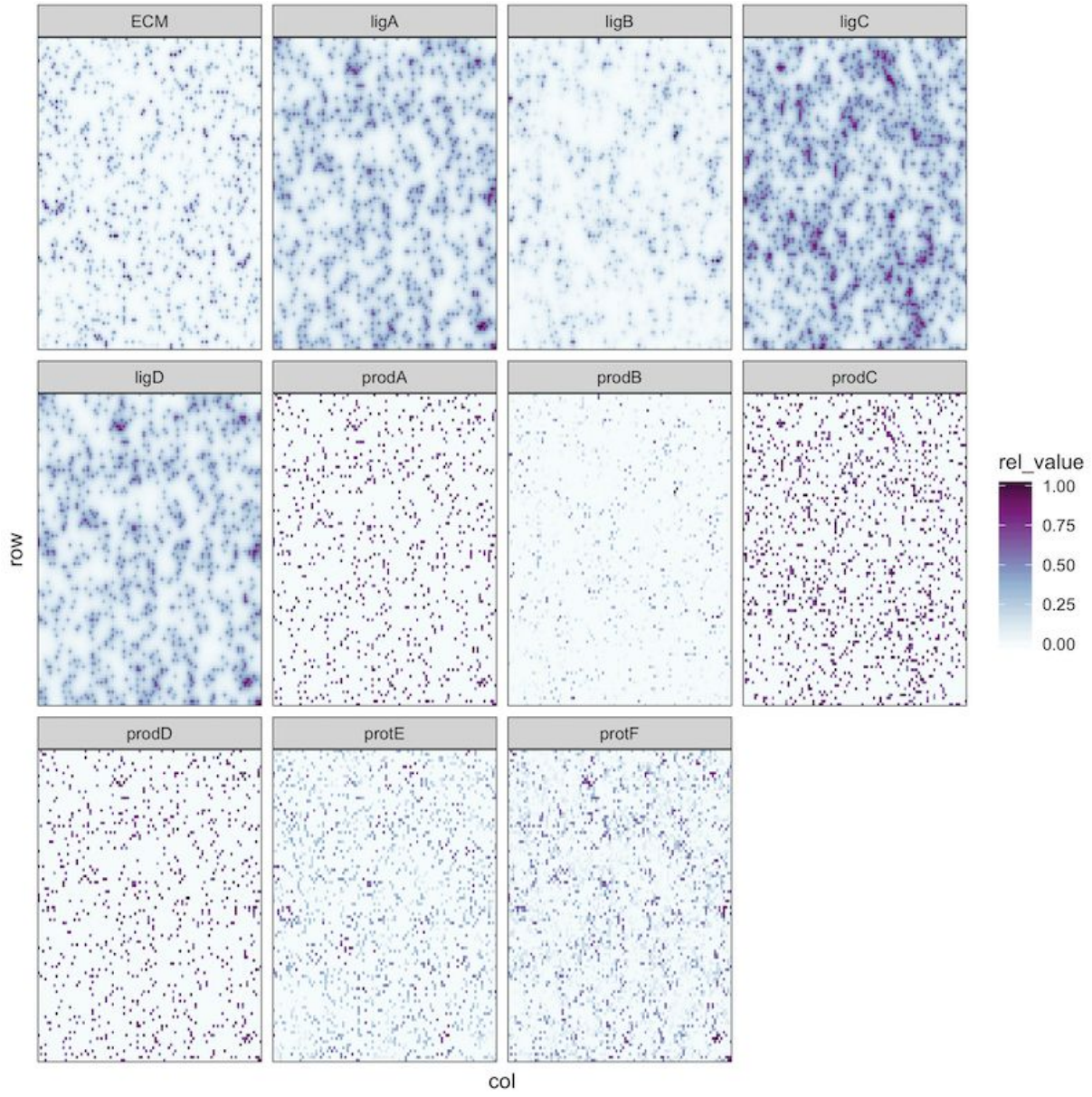

Sup Figure 1. Steady state distribution of simulated species from a single sample.

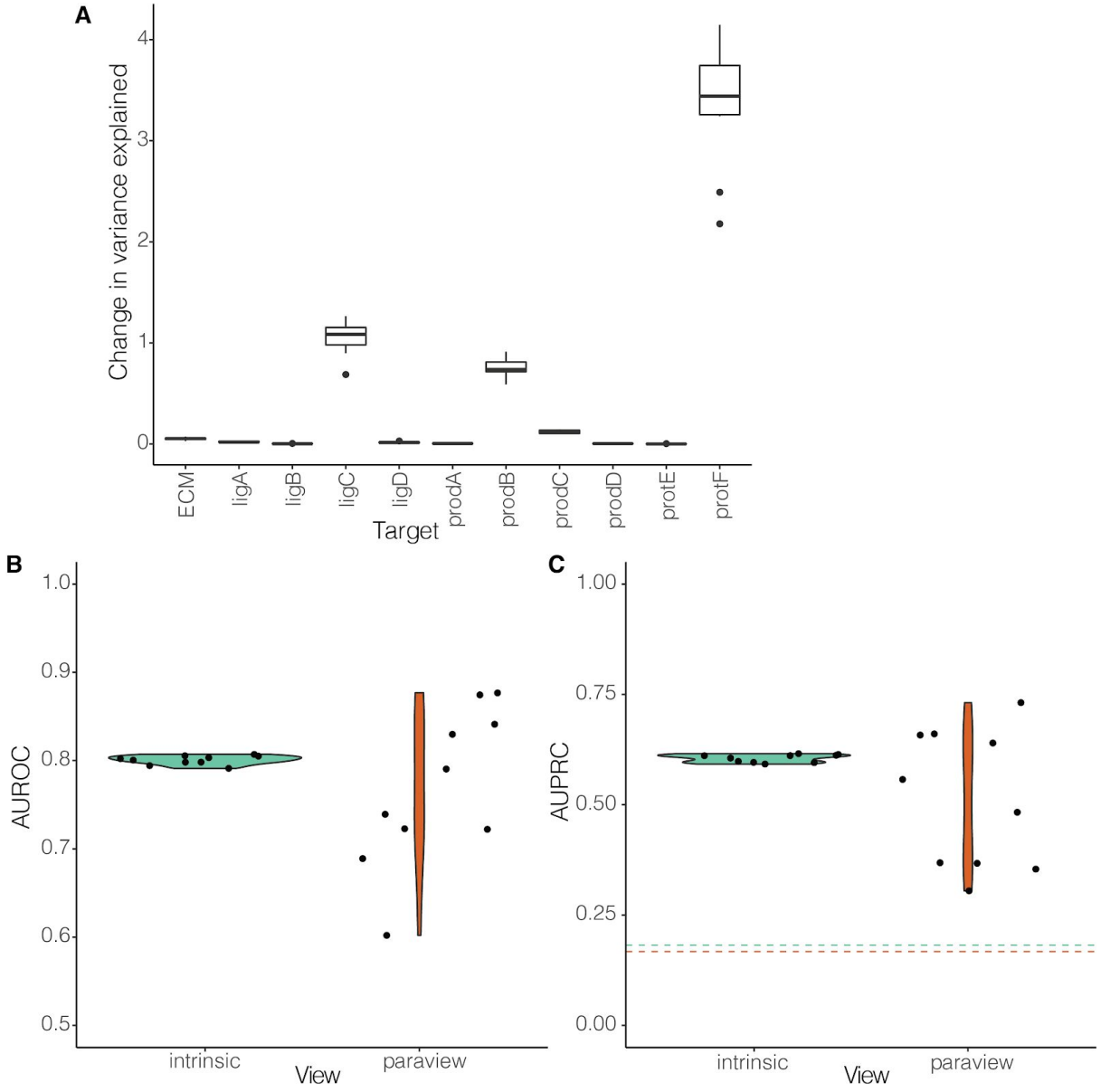

Sup Figure 2. Additional results from the in silico analysis. *(A) Improvement in the predictive performance (variance explained) for all in silico samples when considering multiple views in contrast to a single, intrinsic view. (B) Distribution of AUROC values for the individual samples for the intrinsic and paraview. (C) Distribution of AUPRC values for the individual samples for the intrinsic and paraview.*

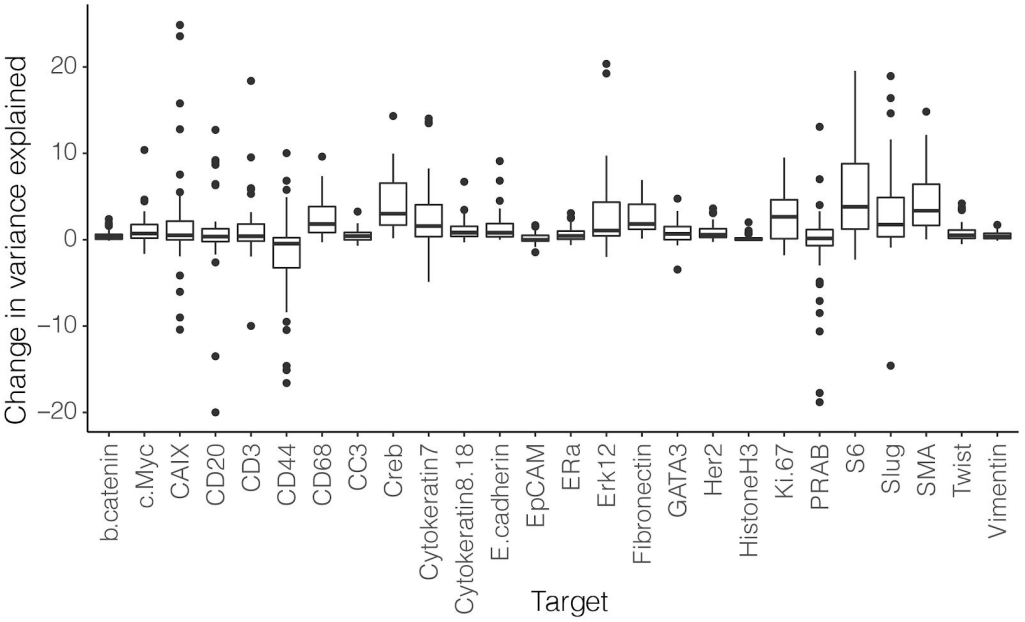

Sup Figure 3. Improvement in the predictive performance (variance explained) for all IMC samples of breast cancer when considering multiple views in contrast to a single, intrinsic view.

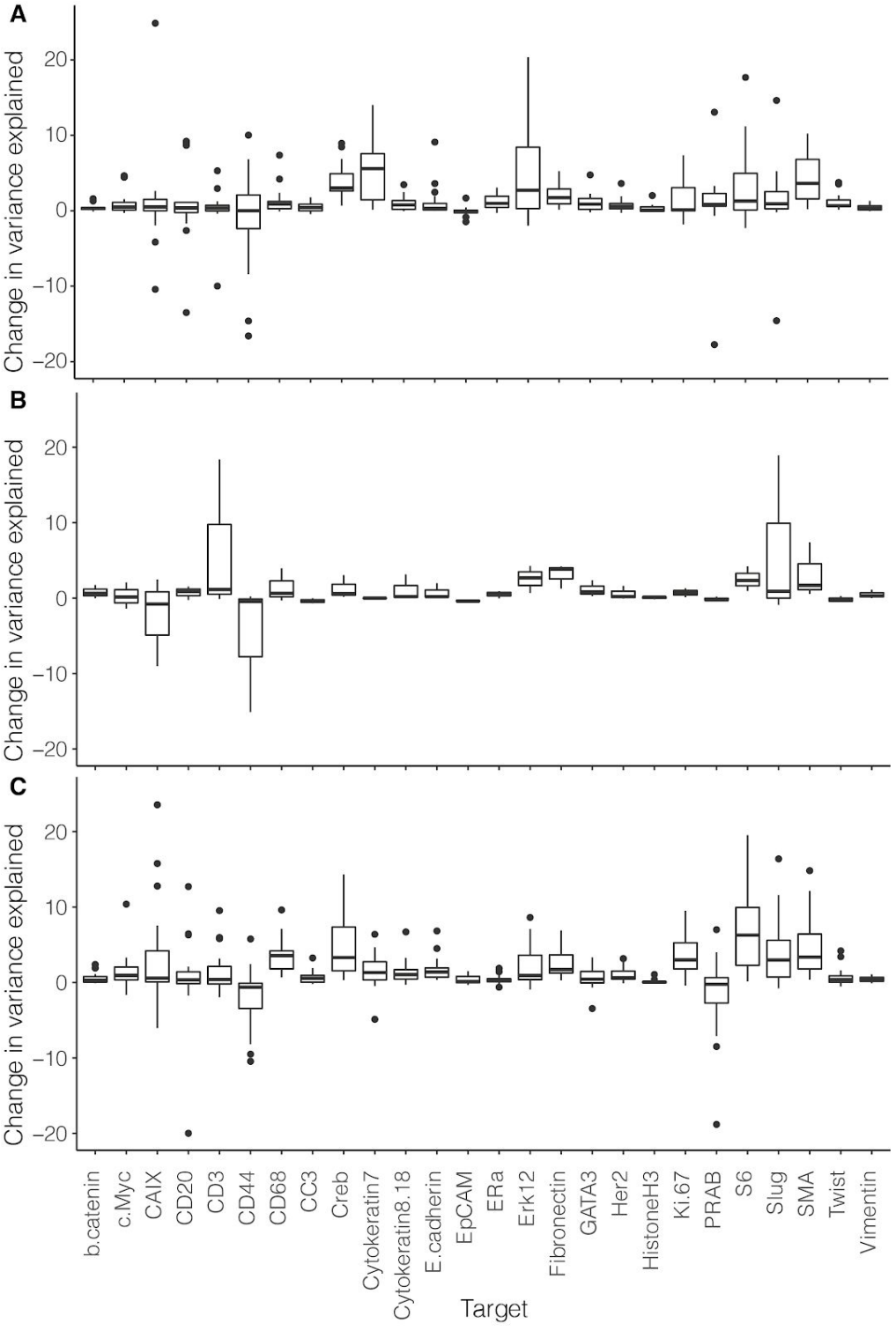

Sup Figure 4. Improvement in the predictive performance (variance explained) for IMC samples of breast cancer by grade when considering multiple views in contrast to a single, intrinsic view. *(A) Grade 1. (B) Grade 2. (C) Grade 3.*

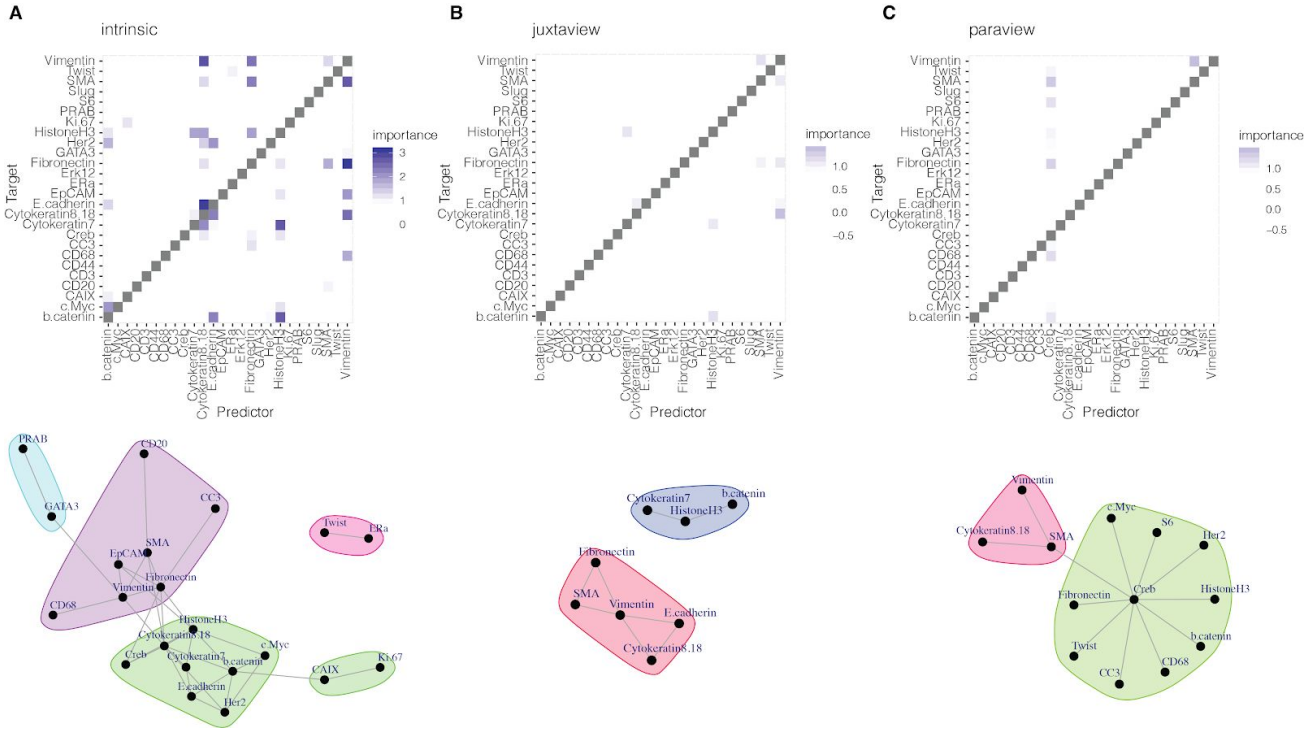

Sup Figure 5. Inferred interactions and communities from IMC grade 1 breast cancer samples.

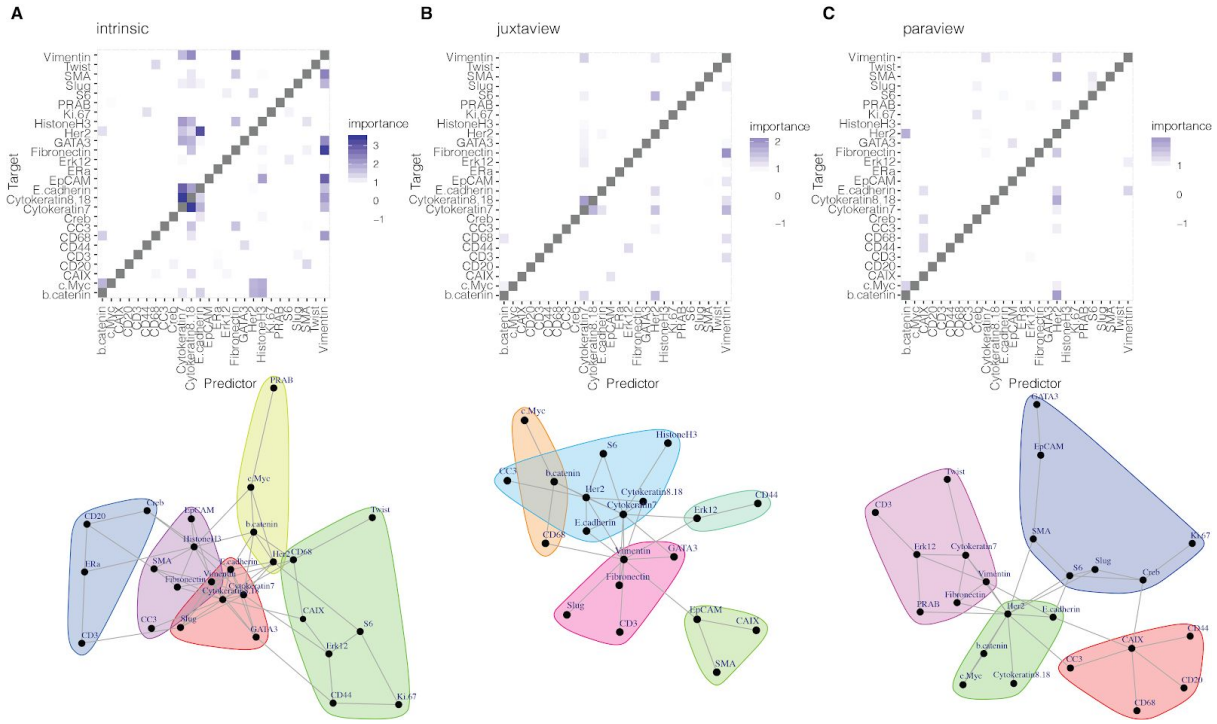

Sup Figure 6. Inferred interactions and communities from IMC grade 2 breast cancer samples.

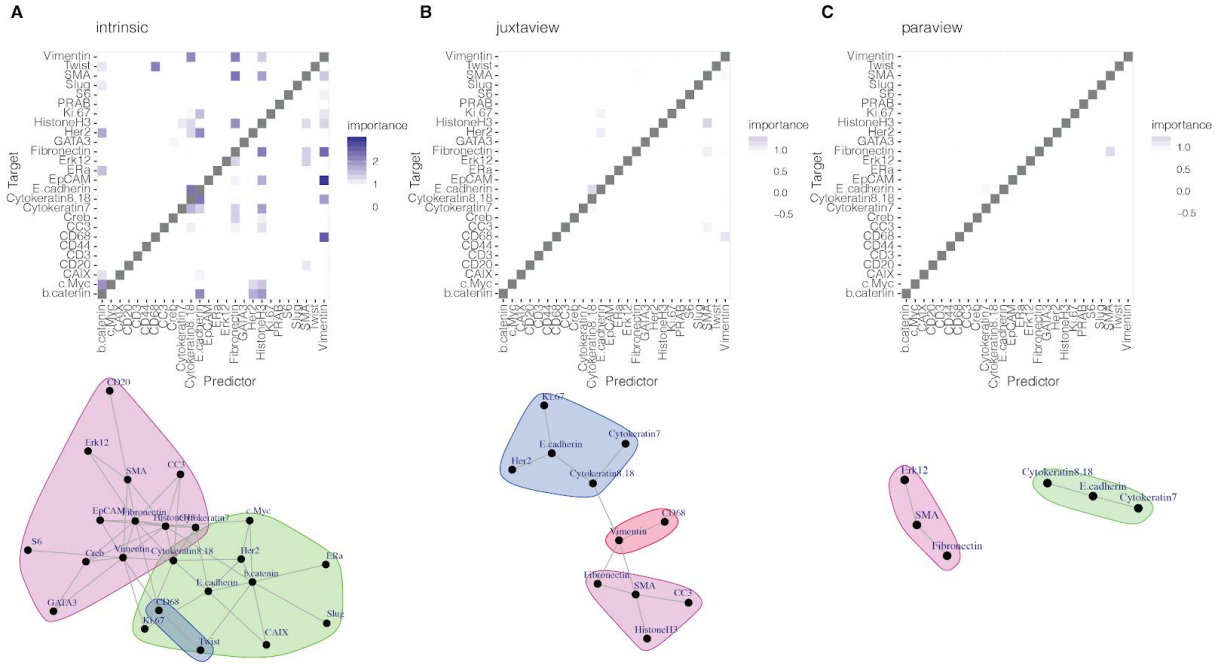

Sup Figure 7. Inferred interactions and communities from IMC grade 3 breast cancer samples.

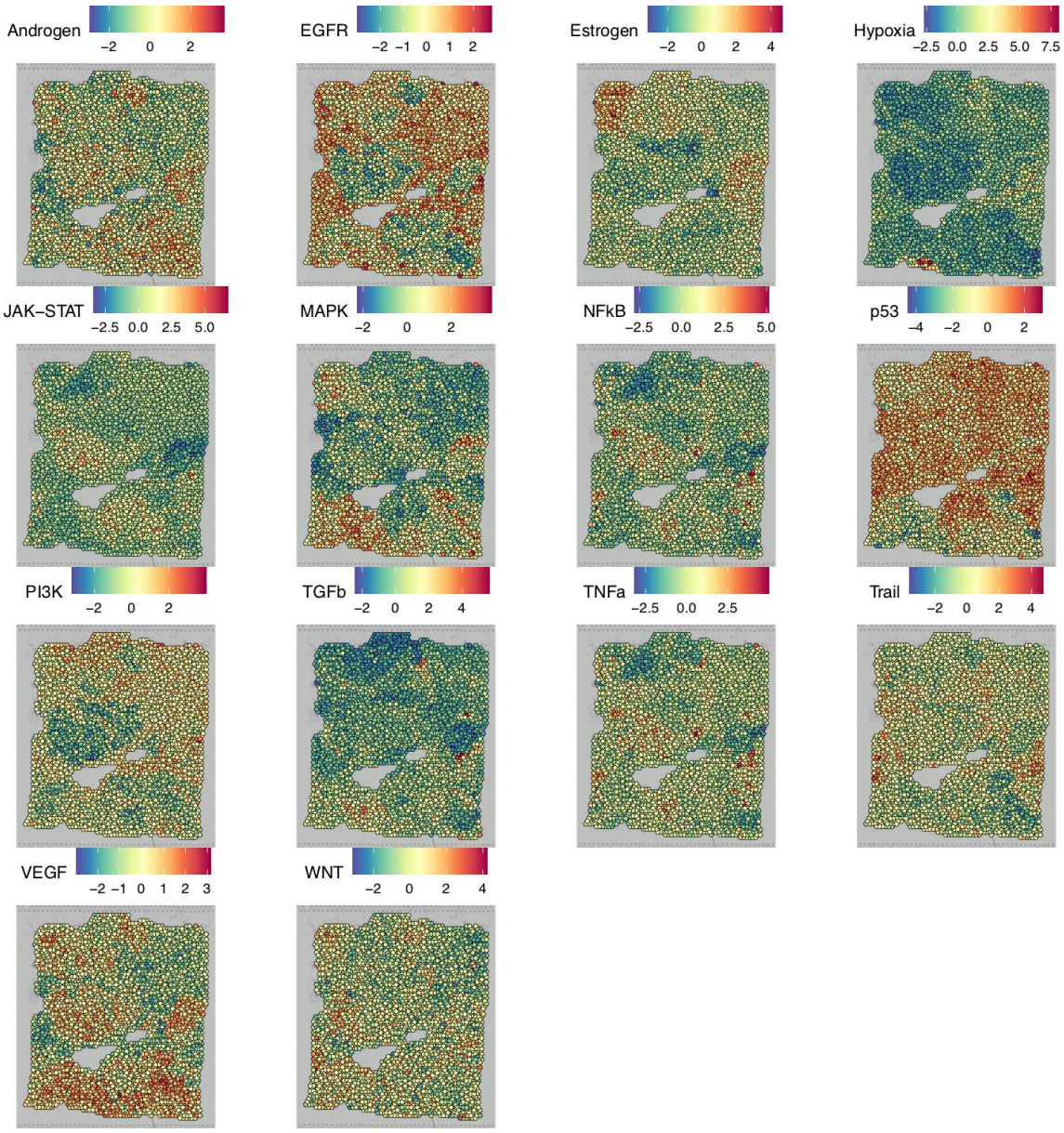

Sup Figure 8. Estimated standardized PROGENy's signaling pathway activities for the first section of a sample of invasive ductal carcinoma in breast tissue profiled with 10x Visium

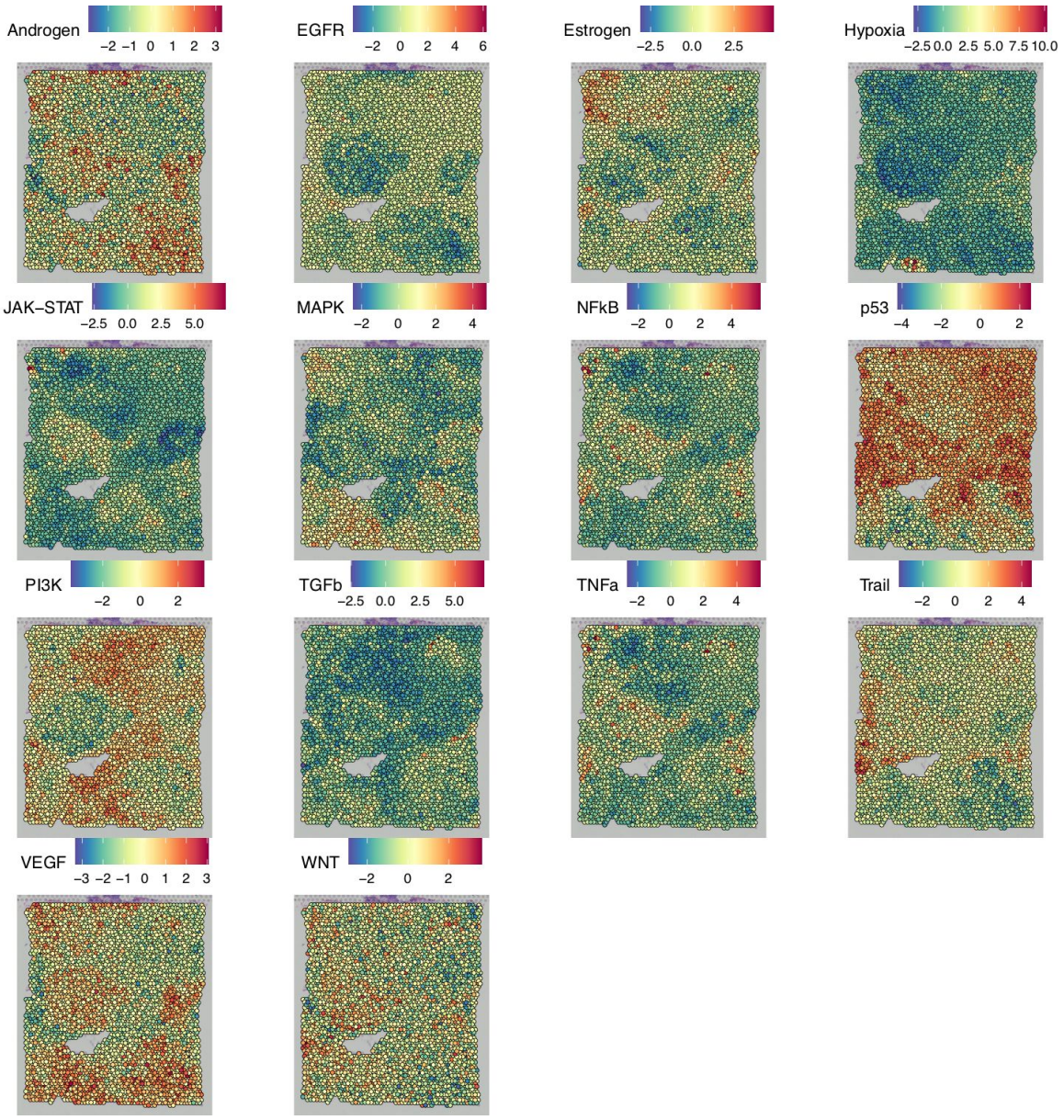

Sup Figure 9. Estimated standardized PROGENy's signaling pathway activities for the second section of a sample of invasive ductal carcinoma in breast tissue profiled with 10x Visium.

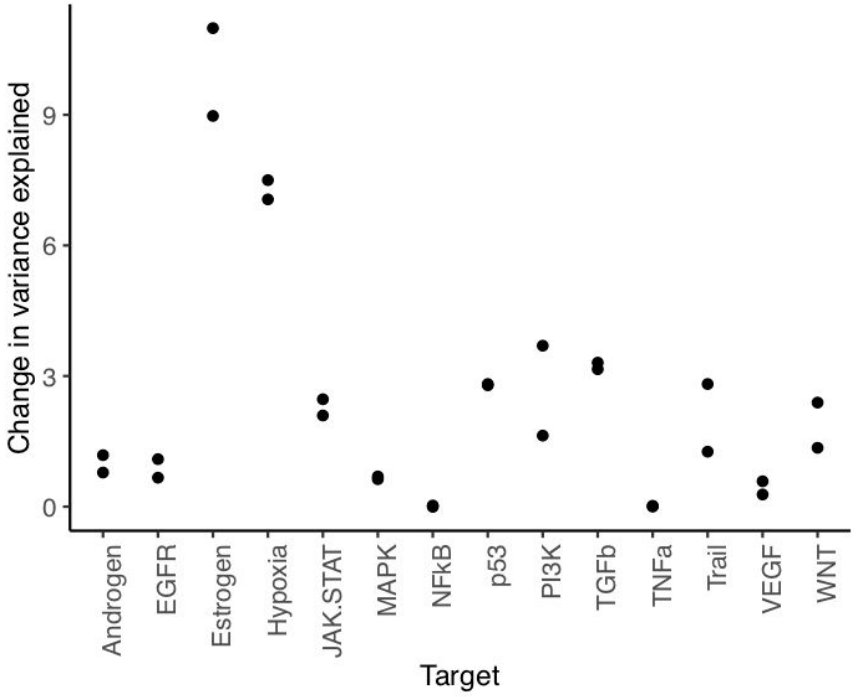

Sup Figure 10. Improvement in the predictive performance (variance explained) of target-pathway specific models when considering multiple views in contrast to a single, intrinsic view.